Carbonization of polysaccharides in FeCl3/BmimCl ionic liquids: Breaking the capacity barrier of carbon negative electrodes in lithium ion batteries

Mohamed Baccour, Nicolas Louvain, Johan Alauzun, Lorenzo Stievano, P. Hubert Mutin, Bruno Boury, Laure Monconduit, Nicolas Brun

Carbonization of Polysaccharides in $FeCl_3$/BmimCl Ionic Liquids: Breaking the Capacity Barrier of Carbon Negative Electrodes in Lithium ion Batteries[1]

Mohamed Baccour,[a,b] Nicolas Louvain,[a,b] Johan G. Alauzun,[a] Lorenzo Stievano,[a,b] P. Hubert Mutin,[a] Bruno Boury,[a] Laure Monconduit,*[a,b] Nicolas Brun*[a]

[a]ICGM, Univ Montpellier, CNRS, ENSCM, Montpellier, France

[b]Réseau sur le Stockage Electrochimique de l'Energie (RS2E), CNRS FR3459, Amiens, France

Abstract

Polysaccharide-derived carbonaceous materials were prepared using an ionothermal carbonization approach in iron-containing ionic liquids (*i.e.* mixtures of 1-butyl-3-methylimidazolium chloride, BmimCl, and iron(III) chloride, $FeCl_3$). The as-prepared ionochars were subsequently pyrolyzed to yield carbon materials. These carbons were thoroughly characterized and investigated as negative electrodes for Li-ion batteries. The use of four polysaccharides (*i.e.* starch, chitosan, pectin and alginic acid) and three different $FeCl_3$/BmimCl ratios allowed obtaining a set of porous carbons with different textural properties (specific surface area and pore volume) and nitrogen contents. Besides, the amount of residual iron within the carbonaceous framework was adjusted through a washing step before pyrolysis, which provided an additional control over the degree of graphitization. The best electrochemical performance in battery was obtained for the carbons prepared from chitosan (*i.e.*, the carbon displaying the highest nitrogen content) and pre-treated in the ionic liquid with the lowest $FeCl_3$/BmimCl ratio (*i.e.*, 0.5, which yielded carbons with higher pore volumes). This work further highlights the versatility offered by the ionothermal approach towards textural, structural and electrochemical properties of the as-prepared carbon materials.

* Corresponding authors. E-mails: laure.monconduit@umontpellier.fr (Laure Monconduit), nicolas.brun@enscm.fr (Nicolas Brun)

1. Introduction

Li-ion batteries (LIBs) occupy in our days a prominent place in a large variety of applications, ranging from portable electronic devices to electric vehicles, to stationary applications. With the advent of next generation cathode materials, expected to yield outstanding high specific capacities (*i.e.* 1675 mAh g^{-1} for sulfur cathodes),[1] the development of negative electrode materials with higher performance is mandatory to replace Li metal electrodes which still present a lot of issues. To date, graphite remains the most used negative electrode material in commercially available LIBs. However, its specific capacity remains relatively low (372 mAh g^{-1}), which might cause an important mismatch with the next generation of positive electrodes. To overcome these downsides, porosity appears as a key parameter. Interconnected and hierarchical pore structures were shown to improve the diffusion of lithium ions, while high specific surface areas promote efficient charge-transfer processes at the electrode-electrolyte interface.[2, 3] Note that such high surface area can also severely impact the efficiency of the first cycle. Different approaches and precursors were developed for the synthesis of advanced porous carbons with high specific surface areas and pore volumes.[3-8] In particular, biosourced porous carbons have attracted increasing interest due to the abundance and the large variety of readily available and often undervalued bioresources.[4] Various routes were developed to transform (carbonize) biomass into porous carbon, such as physical or chemical activation,[9] dry pyrolysis, but also wet pyrolysis in water[10-12] or in less conventional media, for example ionic liquids.[13-15]

Ionic liquids (ILs) have been widely employed for the synthesis of advanced carbonaceous materials, as precursors,[16, 17] porogens,[18] catalysts and/or solvents.[14] Thanks to their easily tunable properties (*e.g.*, viscosity, polarity, and thermal stability), ILs can be seen as designer solvents, especially for the deconstruction and conversion of raw lignocellulosic biomass and biopolymers.[19, 20] This feature has made ILs prime candidate solvents for the preparation of biosourced carbonaceous materials. For instance, 1-butyl-3-methylimidazolium chloride (BmimCl) proved to be highly efficient when used in the solvation of cellulose.[20-22] When mixed with iron(III) chloride ($FeCl_3$), BmimCl yields BmimCl/$FeCl_3$ compounds that display all characteristics of conventional ionic liquids (*i.e.*, high temperature stability, high solvation ability and negligible vapor pressure) together with singular properties such as paramagnetism, moisture-stability and intermediate Lewis acidity.[23] Benefiting from these unique features, Xie *et al.* proposed the use of $BmimFeCl_4$ (obtained from an equimolar mixture of BmimCl/$FeCl_3$) for the thermochemical treatment of

simple saccharides[14, 24, 25] and even raw lignocellulosic biomass.[13] This thermochemical approach, which allows carbonization under mild conditions (*i.e.*, < 10 bars and < 240 °C), has been called ionothermal carbonization (ITC), by analogy with the hydrothermal carbonization (HTC) process. ITC in $BmimFeCl_4$ allowed obtaining carbonaceous materials – called ionochars – with high specific surface areas and high pore volumes. According to the authors, $BmimFeCl_4$ had a multiple role: (i) a porogen; (ii) a Lewis acid catalyst for the carbonization process, and (iii) a recyclable solvent.[14] Besides $BmimFeCl_4$, organic ILs were also employed for the ionothermal treatment of saccharides and raw lignocellulosic compounds.[26] Using Bmim-type ILs with different anions (*i.e.* Cl^-, BF_4^- and Tf_2N^-), Wang *et al.*[26] showed a correlation between the size of the anion and the textural properties of the ionochar – larger anions yielding higher pore volume – further confirming the versatility of the ITC process. Ionochars prepared from various ILs were successfully employed as adsorbents,[24] electrocatalysts[26, 27] and electrode materials for supercapacitors[13, 25].

While full of promise, the ITC process is still a young topic with reaction mechanisms yet to elucidate and a limitless variety of carbon precursor/IL systems to investigate. In this article, we proposed to further explore the ITC process using a set of $BmimCl/FeCl_3$ compounds and polysaccharides for the preparation of carbon negative electrodes in Li-ion batteries (LIBs). The use of four polysaccharides (starch, chitosan, pectin and alginic acid) and three different $FeCl_3$/BmimCl molar ratios (0.5, 1 and 1.5) allowed tuning both textural properties and structural functionalities. We demonstrated a correlation between the ionic structures in $FeCl_3$/BmimCl ILs at different molar ratios and the nanoporosity of the as-prepared ionochars. The amount of residual iron species entrapped within the carbonaceous network was adjusted and provided an additional control over the degree of graphitization. Importantly, the external pore volume and the incorporation of nitrogen functional sites – through the use of chitosan – were identified as important parameters to improve the electrochemical performance of the as-obtained carbons. In this contribution, we wish to show the versatility offered by the ITC process for the synthesis of advanced carbon materials and to produce new insight regarding the use of such materials as negative electrodes in LIBs.

2. Experimental section

2.1. Materials

Alginic acid from brown algae (from Macrocystis pyrifera), pectin from citrus peel (Galacturonic acid ≥74.0 %), chitosan (low molecular weight, 50-190 kDa), starch from potato and N-Methyl-2pyrrolidone (NMP) (anhydrous, 99.5 %) were purchased from Sigma-Aldrich (France). Carboxymethyl cellulose sodium salt (CMC; DS = 0.9, Mw = 250,000) was purchased from Aldrich. Iron (III) chloride hexahydrate was purchased from Acros Organics. 1-Butyl-3-methylimidazolium chloride (99 %) was purchased from Iolitec (Germany). Super P (>99 %) was purchased from Alfa Aesar (France). All reagents were used without further purification.

2.2. Preparation of hydrochars, ionochars and carbon materials

Carbon materials were synthesized by ionothermal carbonization (ITC) of polysaccharides followed by dry pyrolysis under argon. The first step consisted in the thermochemical treatment of polysaccharides in an ionic liquid (IL) in an autoclave, under autogenous pressure. To do so, three $FeCl_3$/BmimCl ILs were prepared by mixing and slightly heating (up to 60 °C) the two components (*i.e.* $FeCl_3$ and BmimCl) at three different $FeCl_3$/BmimCl molar ratios (0.5; 1; and 1.5). As obtained iron-based ionic liquids were then dried at 120 °C under vacuum for 6 hours. Four polysaccharides (*i.e.* chitosan, starch, pectin and alginic acid) were used as carbon precursors. The preparation of the porous carbon materials (**Fig. 1**) consisted in treating 1 g of polysaccharides in 10 mL IL in a Teflon lined stainless steel autoclave (23 mL volume) at 240 °C during 20 h. The as-obtained aromatic carbon networks, called ionochars, were washed twice in demineralised water (50 mL) and once in ethanol (50 mL), filtered with a 0.22 µm PVDF membrane in order to eliminate and recover the IL, and dried in an oven at 80 °C. Ionochars derived from chitosan, starch, pectin and alginic acid were named respectively **CI0.5**, **SI0.5**, **PI0.5** and **AI0.5** when the used IL was prepared with a $FeCl_3$/BmimCl molar ratio of 0.5. In the case of $FeCl_3$/BmimCl molar ratios of 1 and 1.5, ionochars were named respectively **XI1** and **XI1.5** (**X** = **C**, **S**, **P**, **A**). As a comparison, an ionochar was prepared by treating 1 g of starch in 10 mL BmimCl in a Teflon lined stainless steel autoclave (23 mL volume) at 240 °C during 20 h. The resulting material was named **SI0**.

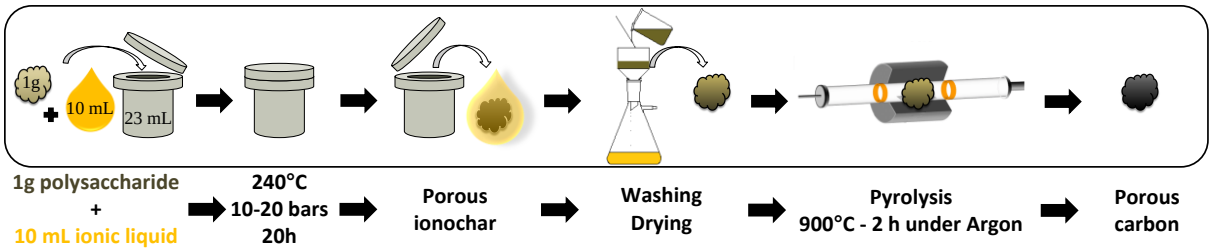

Fig. 1. Schematic representation of the procedure employed to prepare porous carbonaceous materials from the ionothermal carbonization of polysaccharides.

The dried ionochars were pyrolyzed at 900 °C for 2 h with a heating rate of 10 °C min^{-1} under argon flow (45 mL min^{-1}). As-obtained carbon materials were named **XPY** (**X** = **C**, **S**, **P**, **A**; corresponding to the polysaccharide) and (**Y** = **0.5**, **1**, **1.5**; corresponding to the $FeCl_3$/BmimCl molar ratio). An alternative procedure was also applied to ionochars obtained from chitosan with the lowest $FeCl_3$/BmimCl molar ratio (*i.e.*, 0.5). In order to increase the amount of residual iron within the carbonaceous framework, the washing step before pyrolysis was replaced by a simple filtration through a 0.22 µm PVDF membrane without any addition of water or ethanol. After oven-drying and subsequent pyrolysis, the as-obtained carbon was named **CP0.5nw**. **CP0.5nw** was then washed twice in 1 M hydrochloric acid. The as-prepared carbon was named **CP0.5nw-HCl**.

As a comparison, a hydrochar was prepared by treating 1 g of starch in 10 mL water in a Teflon lined stainless steel autoclave (23 mL volume) at 240 °C during 20 h. The dried hydrochar underwent pyrolysis as described previously for ionochars. The resulting carbon material was named **SHP**.

2.3. Characterization

Scanning electron microscopy (SEM) images were obtained using a Hitachi S-4800 electron microscope. Transmission electron microscopy (TEM) images were acquired with a JOEL 1200 microscope. N_2 physisorption experiments were carried out at -196 °C on a Micromeritics 3Flex; ionochars were degassed at 150 °C and carbons (pyrolyzed ionochars) were degassed at 250 °C for 6 h under high vacuum (ca. 0.1 Pa) before physisorption measurements. Raman spectra were acquired on a Horiba Jobin-Yvon LabRAM ARAMIS microspectrometer with an excitation wavelength of 473 nm. XRD patterns were recorded using a PANalytical X'Pert Pro MPD diffractometer, with the Kα radiation of Cu (λ = 1.5418 Å) and a step size of 0.033° into the 10°-70° interval. X-ray photoelectron

spectroscopy (XPS) analyses were performed on a ESCALAB 250 ThermoElectron spectrometer using a monochromatized Al Kα source ($h\nu$ = 1486.6 eV) and a 500 µm spot size. Galvanostatic electrochemical characterizations were carried out at room temperature on a BTS 3000 instrument (Neware Battery).

2.4. Electrode preparation

Electrode slurries with different formulations were prepared using carbonaceous materials derived from polysaccharides as active materials **AM**, Super P as conductive carbon additive **CA** and polyvinylidene fluoride (PVDF) or carboxymethylcellulose sodium salt (CMC; DS = 0.9, Mw = 250,000) as the binder. Three AM:CA:binder weight ratios were used (*i.e.*, 80:10:10, 90:0:10 and 70:18:12). In the case of PVDF, N-methyl-2-pyrrolidone (NMP) was used as solvent, whereas deionised water was used in the case of CMC. Slurries were mixed using an agate grinding jar containing four 4 mm diameter agate balls. A Fritish Pulverisette 7 was used to mill the mixture at 500 rpm for 1 h and then the slurry was tape casted uniformly at 150 µm onto 18 µm thick copper current collector. Electrodes with a diameter 12.7 mm were cut using a disk cutter and dried under vacuum for 6 h at 80 °C. Coin cells were assembled under Ar atmosphere (O_2 < 0.5 ppm, H_2O < 0.5 ppm) in glove box (MBraun). Lithium metal was used as reference and counter electrode. The electrolyte used was LP30 (1M $LiPF_6$ dissolved in a mixture of ethylene carbonate (EC) and dimethyl carbonate (DMC) (EC:DMC = 1:1). Whatman glass fiber disk were used as separators. The electrochemical galvanostatic measurements were carried out in the voltage of 3.00-0.01 V versus Li^+/Li at different current densities.

3. Results and discussion

3.1. Ionochars and ionochar-derived carbons

Carbon materials were synthesized in a three-step procedure as described in **Fig. 1**: (i) ionothermal carbonization (ITC) of polysaccharides in $FeCl_3$/BmimCl ILs, (ii) separation of the as-obtained ionochars, and (iii) pyrolysis under argon flow at 900 °C to obtain porous carbons. The first step, so-called ITC, is a thermochemical process which allows carbonization of (poly)saccharides under mild conditions (*i.e.* < 10 bars and < 240 °C) and proceeds in a similar way as hydrothermal carbonization (HTC).[28, 29] Therefore, the conversion of polysaccharides into ionochars is assumed to proceed in three main steps: (i) hydrolysis into monosaccharide units, (ii) dehydration of monosaccharides into furan

derivatives, and (iii) polycondensation of furan derivatives into polyfuranic species.[4, 28-30] At high temperature, typically at 240 °C as described here, the carbonization process continues *via* intramolecular reactions (*i.e.*, condensation, dehydration and decarbonylation reactions) which lead to the production of condensed polyaromatic domains. At that stage, it is important to notice that ITC occurs under autogenous pressure induced by water produced during dehydration/condensation reactions and by low-boiling point organic by-products. ITC of carbohydrates in $BmimFeCl_4$ was previously described by Xie *et al.*, and the key role of this IL was clearly evidenced.[14] $FeCl_3$ acts as a Lewis acid catalyst involved in the different stages of the carbonization process. Its combination with BmimCl yields a room-temperature IL which acts as a porogen and as a solvent with superior solvation properties compared with water. Thus, ITC of carbohydrates in $BmimFeCl_4$ generates porous ionochars with a higher carbonization yield compared with analogous hydrochars obtained by the HTC process.

Herein, ionochars were synthesized from four polysaccharides – chitosan (**C**), starch (**S**), pectin (**P**) and alginic acid (**A**) in $BmimFeCl_4$. The nitrogen sorption isotherms and textural properties of the four corresponding ionochars are presented in **Figure S1**. Significant differences were observed depending on the polysaccharide. While ionochars derived from pectin (**PI1**) and alginic acid (**AI1**) display type-I isotherms related to microporous materials, starch-derived ionochar (**SI1**) displays a type I/II isotherm with a H3 hysteresis loop, related to micro-macroporous materials.[31] A slight H4 hysteresis loop was observed for AI1, suggesting the presence of slit-like mesopores. Unlike the three other polysaccharides, chitosan yielded a nonporous ionochar (**CI1**; **Fig. S1**). As mentioned previously, $BmimFeCl_4$ is supposed to act as a porogen and as a catalyst during the ITC process. This feature was demonstrated by comparing a hydrochar obtained from starch through HTC in water (**SH**), an ionochar obtained from starch through ITC in BmimCl (**SI0**) and the analogous obtained through ITC in $BmimFeCl_4$ (**SI1**). While **SI1** displays a BET equivalent specific surface area (SSA) of 200 $m^2\ g^{-1}$ and a mass yield of 50 wt.% (**Table S1**), both **SH** and **SI0** are non-porous and present lower mass yields (36 and 38 wt.%, respectively, **Table S1**).

After pyrolysis at 900 °C, the shapes of isotherms and the hysteresis loops were preserved for **PP1**, **AP1** and **SP1** (**Fig. 2a**). A significant increase in SSA, inherent to the self-activation process directed by the gases produced during pyrolysis, was noticed for each sample (**Table 1**). This feature was also observed for the carbon derived from chitosan (**CP1**), which displays a type-I isotherm (**Fig. 2a**). While **SHP** and **SP1** display similar SSAs and micropore volumes (**Table 1**), **SP1** displays a higher external pore volume due to the

contribution of large mesopores and/or narrow macropores. The textures observed by SEM (**Fig. 3**) are in good agreement with the nitrogen physisorption data. Smooth surfaces were observed for the microporous carbons (**PP1**, **AP1** and **CP1**), while a meso-macroporous structure made of aggregated nanoparticles was obtained for the starch-derived carbon (**SP1**). Larger particles, typical of HTC-derived carbons, were observed for **SHP** (**Fig. 3a**). Micrometric hollow spheres were observed for the pectin derived materials (**Fig. 3c**), suggesting supramolecular self-assemblies between pectin and imidazolium cations.

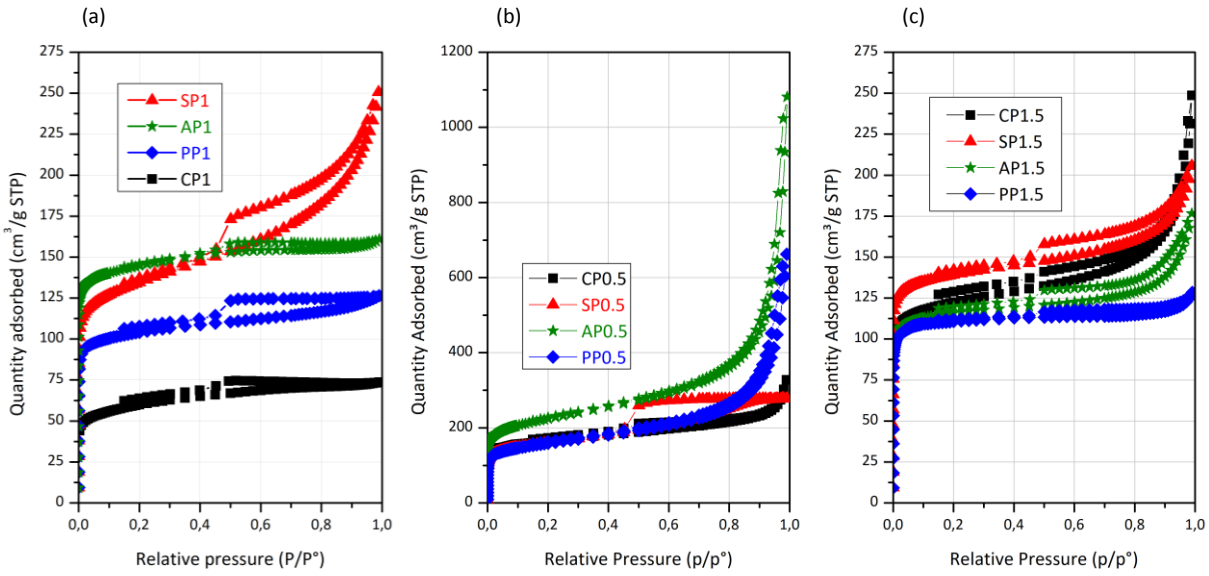

Fig. 2. N_2 physisorption isotherms of carbon materials prepared in this study.

Besides the equimolar $FeCl_3$/BmimCl mixture, two other $FeCl_3$/BmimCl molar ratios, 0.5 and 1.5, were used for the ITC of the four polysaccharides. The nitrogen sorption isotherms of the as-prepared carbons after pyrolysis are shown in **Fig. 2b** (ratio 0.5) and **Fig. 2c** (ratio 1.5), and the corresponding textural properties are reported in **Table 1**. For each polysaccharide, both SSA and pore volume (especially external pore volume) reached a maximum for the lowest $FeCl_3$/BmimCl molar ratio (*i.e.*, 0.5). In a recent study, Li *et al.*[32] observed the formation of nanostructures in $FeCl_3$/BmimCl ILs at different molar ratios. The sizes of the local domains were found to be tens of nanometers. Interestingly, the authors showed that the compactness and the thermal stability of the nanostructures in $FeCl_3$/BmimCl ILs were significantly higher when decreasing the $FeCl_3$/BmimCl molar ratio from 1 to 0.6. These features were explained based on the stronger inter-ionic interactions in ILs with lower $FeCl_3$/BmimCl molar ratios, *i.e.*, when Cl^- and $FeCl_4^-$ coexist. Li *et al.*[32] further supported this statement by comparing conductivities and glass transition temperatures. In our study,

carbons obtained in ILs displaying nanostructures with higher compactness and higher thermal stability (*i.e.*, molar ratio of 0.5) exhibit higher SSA and higher external pore volume (**Table 1**). Thus, ionic structures in $FeCl_3$/BmimCl ILs appear as a critical factor that might impact supramolecular assemblies during the ITC process and tune, *in fine*, the nanoporosity of carbons.

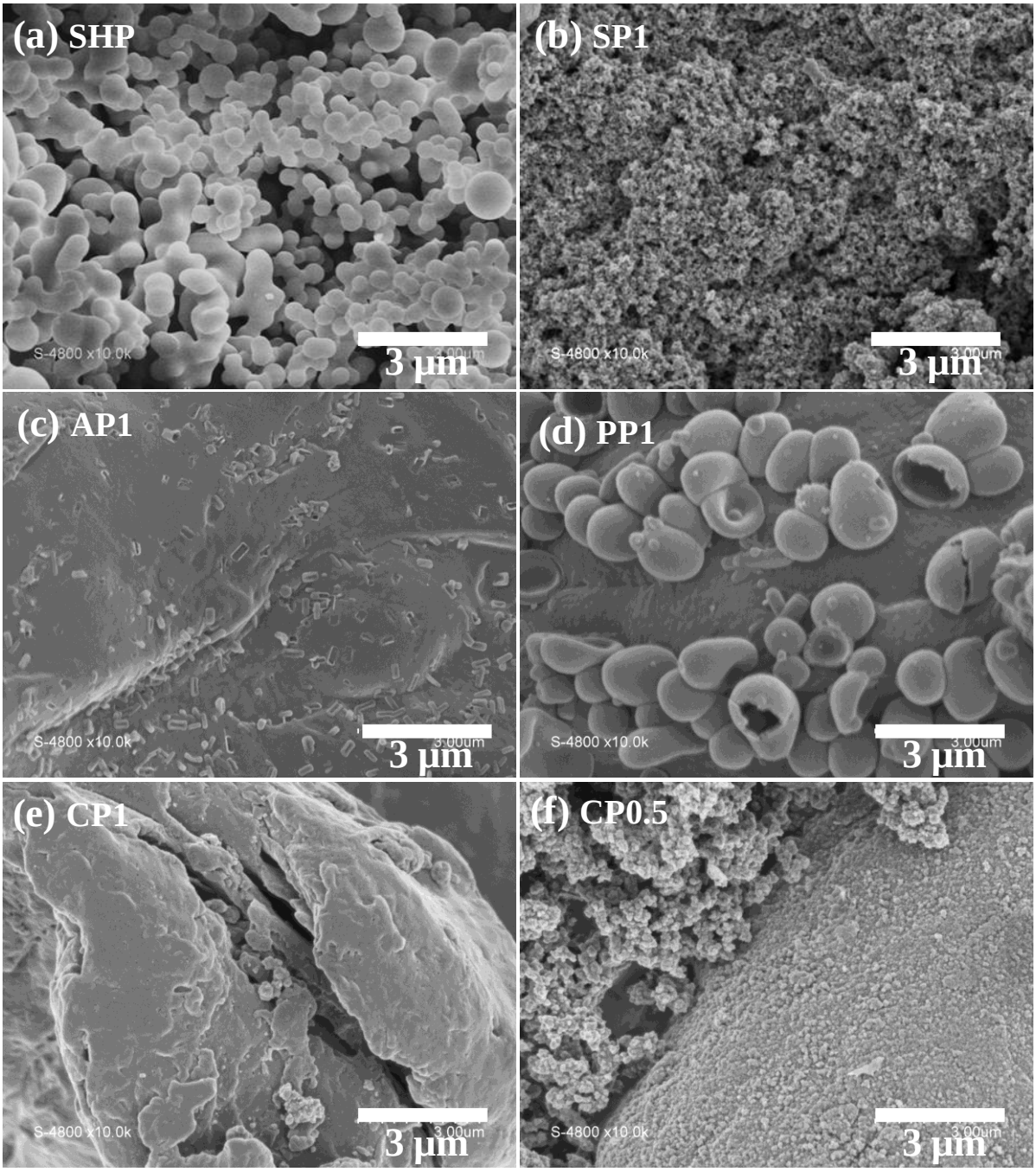

Fig. 3. SEM images of carbon materials obtained via HTC of starch (SHP), and via ITC in a 1:1 $FeCl_3$/BmimCl IL of starch (SP1), alginic acid (AP1), pectin (PP1), chitosan (CP1) and in a 0.5:1 $FeCl_3$/BmimCl IL of chitosan (CP0.5).

Table. 1: Textural properties of the carbon materials prepared in this study. [†]BET Specific Surface Area (SSA); [‡]Total pore volume determined at P/P_0 0.95 (adsorption); [ϕ]Micropore and external pore volumes determined by the t-plot method.

Samples	SSA[†] ($m^2\ g^{-1}$)	Pore volume[‡] ($cm^3\ g^{-1}$)	Micropore volume[ϕ] ($cm^3\ g^{-1}$)	External pore volume[ϕ] ($cm^3\ g^{-1}$)
SP0.5	590	0.43	0.14	0.29
SP1	510	0.36	0.15	0.21
SP1.5	545	0.29	0.19	0.10
SHP	430	0.17	0.17	0
AP0.5	820	1.00	0.20	0.80
AP1	575	0.24	0.22	0.02
AP1.5	455	0.25	0.17	0.08
PP0.5	580	0.77	0.15	0.62
PP1	410	0.20	0.15	0.05
PP1.5	440	0.19	0.17	0.02
CP0.5	620	0.40	0.20	0.20
CP1	220	0.11	0.09	0.02
CP1.5	475	0.30	0.16	0.14
CP0.5nw	145	0.29	0.02	0.27
CP0.5nw-HCl	195	0.32	0.06	0.26

Besides nanoporosity, the influence of ITC and $FeCl_3$/BmimCl molar ratio over the carbon microstructure was investigated by Raman spectroscopy. **Fig. 4a** shows the Raman spectra for the four carbon materials obtained in IL with a $FeCl_3$/BmimCl molar ratio of 1. D and G bands can be observed at 1345 and 1583 cm^{-1}, respectively. Also, two broad peaks were observed in the 2650 to 3150 cm^{-1} region. They are related to the 2D (2690 cm^{-1}) and D + G bands (2960 cm^{-1}) of carbonaceous materials, and are typical of disordered pseudo-graphitic structures with a low level of graphitization. Carbon materials derived from starch and prepared by ITC in $FeCl_3$/BmimCl ILs with 0.5, 1 and 1.5 molar ratios were compared to an analogous starch-derived carbon prepared by HTC in pure water. The obtained Raman spectra of all the carbons were similar (**Fig. 4b**), showing that neither ITC (as compared with HTC, see sample SHP), nor the $FeCl_3$/BmimCl molar ratio affected the degree of graphitization after pyrolysis. The same feature was observed for the other polysaccharide-derived carbons. This behavior can be explained by the low concentration and/or heterogeneous dispersion of the residual iron species embedded in the ionochars (**Table 2**). In fact, after ITC, the ionochars were thoroughly washed with water and ethanol, to remove $FeCl_3$/BmimCl before pyrolysis. In order to increase the amount of residual IL (and the amount of residual iron) within the carbonaceous framework, the washing step before pyrolysis was replaced by a short filtration without any addition of water or ethanol. This experiment was performed with chitosan in IL with a $FeCl_3$/BmimCl molar ratio of 0.5 (sample named **CP0.5nw**). The amount of residual iron in **CP0.5nw** was significantly increased as compared with **CP0.5**; the proportion of iron estimated by SEM-EDX was 4.5 at.% in **CP0.5nw** against 0.17 at.% in **CP0.5** (**Table 2**). The presence of residual iron during pyrolysis affected both the nitrogen content (**Table 2**) and the textural properties (**Fig. 5a** and **Table 1**). While **CP0.5** displays a type I/II isotherm with a H3 hysteresis loop, **CP0.5nw** displays a type I/II isotherm with a H2(a) hysteresis loop. This H2(a) hysteresis loop is ascribed to pore-blocking effects and cavitation-induced evaporation of nitrogen trapped in pores connected by narrow necks. Moreover, **CP0.5nw** displays a lower pore volume and a lower SSA as compared with **CP0.5**. As shown in **Fig. 5b**, significant differences were also observed by Raman spectroscopy. As for **CP0.5nw**, the G band is thinner and is significantly more intense than the D band. The I_D/I_G ratio decreases from 0.8 for **CP0.5** to 0.34 for **CP0.5nw**, suggesting a higher degree of graphitization in **CP0.5nw**. The microstructure of carbons derived from chitosan was further investigated by XRD. XRD patterns (**Fig. 5c**) showed a broad and non-intense signal centered at about 26° for **CP0.5**,

CP1 and **CP1.5**, which corresponds to the reflection of carbon atoms in the (002) plane. This feature is in good agreement with Raman spectroscopy and confirms that these three samples are amorphous. On the contrary, the peak centered at 26° is more intense and narrower for **CP0.5nw**, suggesting a better orientation of the aromatic carbon layer slices and a higher degree of graphitization, as already supported by Raman spectroscopy. Besides the peak associated with carbon, **CP0.5nw** shows several reflection peaks between 42° and 47° typical of iron carbide, Fe_3C (**Fig. S2**). The intense reflection peak centered at 44.5° and the weak reflection peak centered at 65° also suggest the presence of Fe(0) in this sample. The carbothermal reduction of iron salts to iron carbide at high temperature is well known and was already described in ITC processes by Taubert *et al.* starting from $BmimFeCl_4$.[14, 33] The presence of Fe(0) in Fe_3C was also reported.[33] The treatment of **CP0.5nw** in HCl yielded **CP0.5nw-HCl** and allowed the partial removal of the iron species. In the XRD pattern of **CP0.5nw-HCl**, the reflection peaks related to Fe_3C were less intense (**Fig. 5c**) and the reflection peaks related to Fe(0) totally vanished (**Fig. S2**).

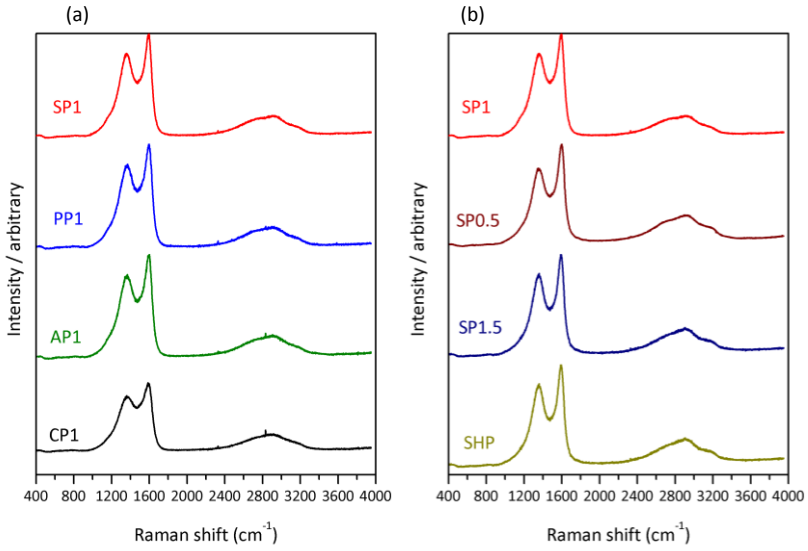

Fig. 4. Raman spectra of carbon materials **(a)** derived from four polysaccharides by ionothermal carbonization in IL with molar ratio $FeCl_3$/BmimCl = 1 and **(b)** derived from starch and carbonized in different ILs and water.

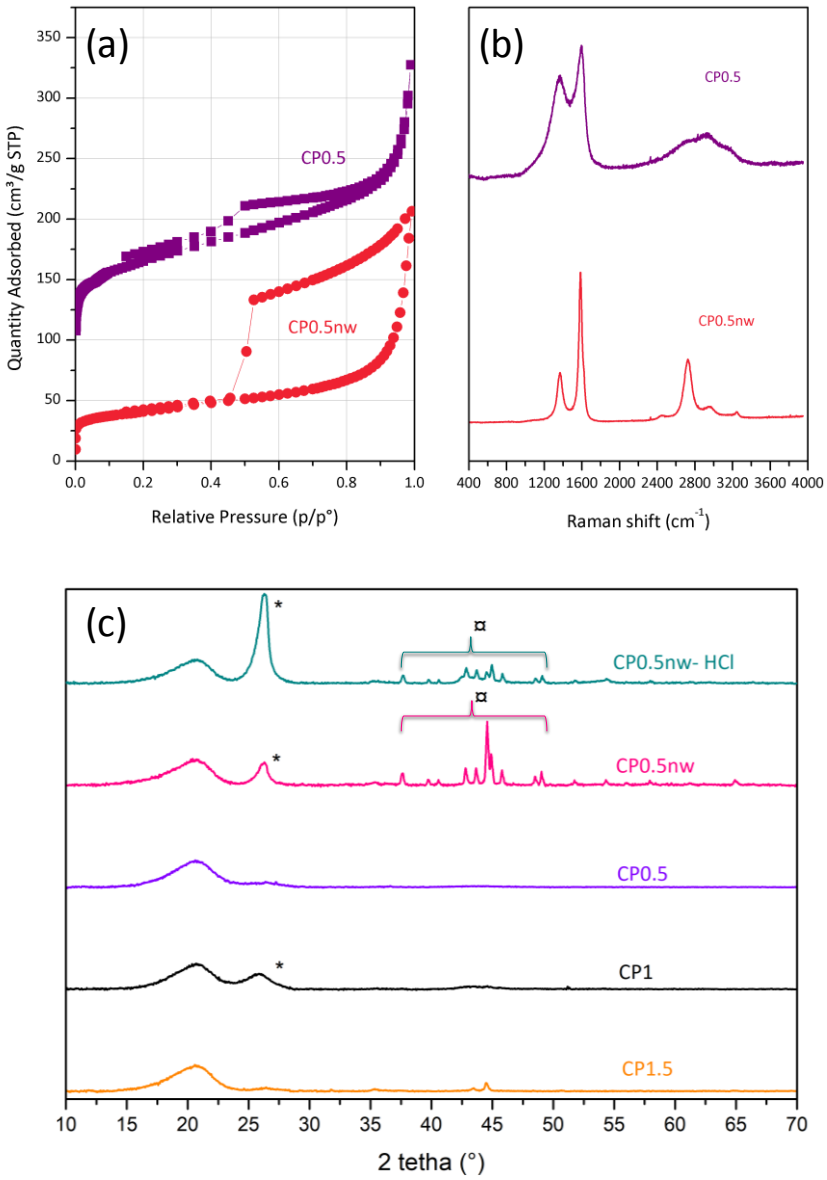

Fig. 5. (a) N_2 physisorption isotherms and **(b)** Raman spectra of **CP0.5** (0.17 at.% Fe)‡ and **CP0.5nw** (4.5 at.% Fe)‡. **(c)** X-ray powder diffraction patterns of the five carbons derived from chitosan: **CP0.5** (0.17 at.% Fe)‡, **CP0.5nw** (4.5 at.% Fe)‡, **CP0.5nw-HCl** (1.0 at.% Fe)‡, **CP1** (0.45 at.% Fe)‡ and **CP1.5** (2.6 at.% Fe)‡ .‡Iron contents according to SEM-EDX. X-ray diffraction profiles assigned to graphite [26-1079] (*); and Fe_3C [01-085-1317] (¤). The intense reflection centered at 44.5°, mainly present in **CP0.5nw**, can be assigned to Fe_3C (left shoulder or section of the reflection) and Fe(0). The reflection at 65°, mainly present in **CP0.5nw**, can be assigned to Fe(0).[33]

Table 2. Weight proportion of nitrogen, N/C atomic ratio and atomic proportion of iron of the carbon materials used in this study. $^{\phi}$XPS; †Elemental analysis; ‡SEM-EDX.

Samples	N/C (at.)$^{\phi}$	N (wt.%)†	Fe (at.%)
CP1.5	0.017	2.0	2.6‡ (0.09)$^{\phi}$
CP1	0.032	4.7	0.45‡ (0.09)$^{\phi}$
CP0.5	0.029	4.4	0.17‡ (n/a)$^{\phi}$
CP0.5nw	0.018	0.2	4.5‡ (0.58)$^{\phi}$
CP0.5nw-HCl	0.016	-	1.0‡ (0.57)$^{\phi}$

These observations were confirmed by TEM. As shown in **Fig. 6a**-**b**, **CP0.5** is mainly amorphous and no iron-containing particles could be identified, while **CP0.5nw** presents a snail-like graphitic carbon structure surrounding iron-based particles. These snail-like graphitic carbon structures were also observed by high resolution TEM (**Fig. 6c**), and graphitic plans were clearly identified. The profile of intercross distance (**Fig. 6d**) gave a plan-to-plan distance of about 0.34 nm, which corresponds to the distance between carbon layers in graphite.

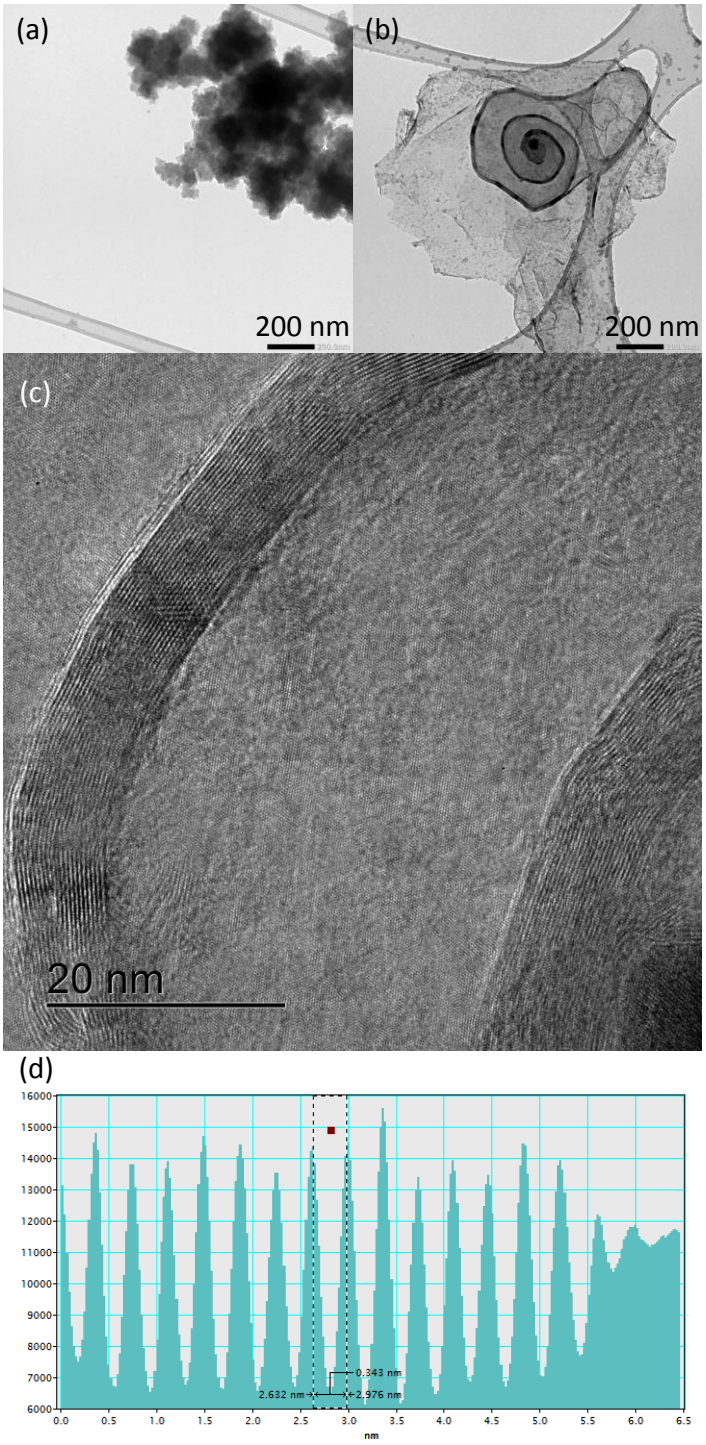

Fig. 6. TEM images for **(a) CP0.5** (0.17 at.% Fe)‡ and **(b) CP0.5nw** (4.5 at.% Fe)‡. **(c)** High-resolution TEM images for **CP0.5nw** and **(d)** profile of intercross distance. ‡According to SEM-EDX.

3.2. Electrochemical performance as negative electrodes in lithium ion batteries

The different carbon materials synthesized in this study were tested as active materials (**AM**) for the preparation of negative electrodes in Li-ion batteries. The four polysaccharide-derived

carbons based electrodes (see the electrode preparation in the experimental part) treated in IL with a $FeCl_3$/BmimCl molar ratio of 1 were compared by galvanostatic charge-discharge measurements (**Fig. S3** and **Table 3**). As shown in **Table 3**, the first discharge capacities are 741, 634, 602 and 498 mAh g^{-1} for SP1, CP1, AP1 and PP1, respectively. All samples show a low coulombic efficiency (CE) for the first cycle: 38, 51, 44 and 50 % for SP1, CP1, AP1 and PP1, respectively. This poor CE is often correlated with the high surface area of the **AM** which promotes the irreversible degradation of the electrolyte and the formation of a solid electrolyte interphase (SEI). After about ten cycles, all samples show a stabilization of both capacity (270, 289, 245 and 231 mAh g^{-1}) and coulombic efficiency (97, 98, 98 and 99 % for SP1, CP1, AP1 and PP1, respectively), with a good stability over 50 cycles (See **Table 3**). The electrode derived from chitosan (**CP1**) presents the highest capacity. This result can be explained by the presence of nitrogen coming from chitosan (4.4 wt.% as shown in **Table 2**). In fact, pyridinic and quaternary nitrogen atoms are expected to improve electronic conductivity and to introduce more defects and active sites in carbon frameworks, enhancing both lithium storage capacity and rate capability in carbon-based negative electrodes.[34] At that stage, it is important to note that the carbons obtained from starch (**SP1**), pectin (**PP1**) and alginic acid (**AP1**) display low nitrogen contents (≤ 1.0 wt.% according to elemental analyses), coming most probably from the presence of residual imidazolium moieties. In a previous study, Kim *et al.*[3] showed that the mesoporosity and the intrinsic electronic conductivity are two very important parameters when dealing with carbon-based negative electrodes for LIBs. Based on our results, nitrogen content seems to prevail over mesoporosity, as the specific capacity of **SP1** – the sole mesoporous carbon of the series – is significantly lower as the one of **CP1** (**Table 1**).

Table 3. Capacities and coulombic efficiency at the 1st, 10th, and 50th cycles for carbons derived from polysaccharides and treated in IL ($FeCl_3$/BmimCl = 1)

Sample	Discharge capacity at 1st cycle (mAh g^{-1})	Reversible capacity (mAh g^{-1})			Coulombic efficiency (%)		
		at 1st cycle	at 10th cycle	at 50th cycle	at 1st cycle	at 10th cycle	at 50th cycle
SP1	741	294	270	263	38	97	98
CP1	634	323	289	280	51	98	100

AP1	602	265	245	242	44	98	99
PP1	498	247	231	235	50	99	99

The influence of the IL (*i.e.*, the $FeCl_3$/BmimCl molar ratio) used during ITC over the electrochemical performance was assessed for the materials obtained from starch (**Fig. 7a**), chitosan (**Fig. 7b**), pectin (**Fig. 7c**) and alginic acid (**Fig. 7d**). For all polysaccharides, a clear trend can be emphasized. **SP0.5**, **CP0.5**, **PP0.5** and **AP0.5**, which are the samples with the largest external pore volume of their respective series (**Table 1**), present the highest reversible specific capacity (between 400 and 450 mAh g^{-1} at first cycle). As for the carbons derived from starch, pectin and alginic acid (*i.e.*, the nitrogen-free polysaccharides), a clear correlation was observed between the external pore volume and the specific capacity (**Table 1** and **Fig. 7**). Unlike these three polysaccharides, the external pore volume cannot be seen as the sole key parameter to impact the specific capacity of the chitosan-derived carbons. While **CP1.5** displayed a higher external pore volume (0.14 cm^3 g^{-1}) than **CP1** (0.02 cm^3 g^{-1}), **CP1** clearly showed a higher specific capacity (**Fig. 7b**). As mentioned above, the nitrogen content seems to prevail over mesoporosity. This statement was confirmed also in this case, since **CP1.5** has a lower nitrogen content than **CP1** (**Table 2**), probably due to the larger amount of residual iron which appears to be responsible for nitrogen removal during pyrolysis.[35] This behavior was also confirmed with **CP0.5nw** (**Table 2**).

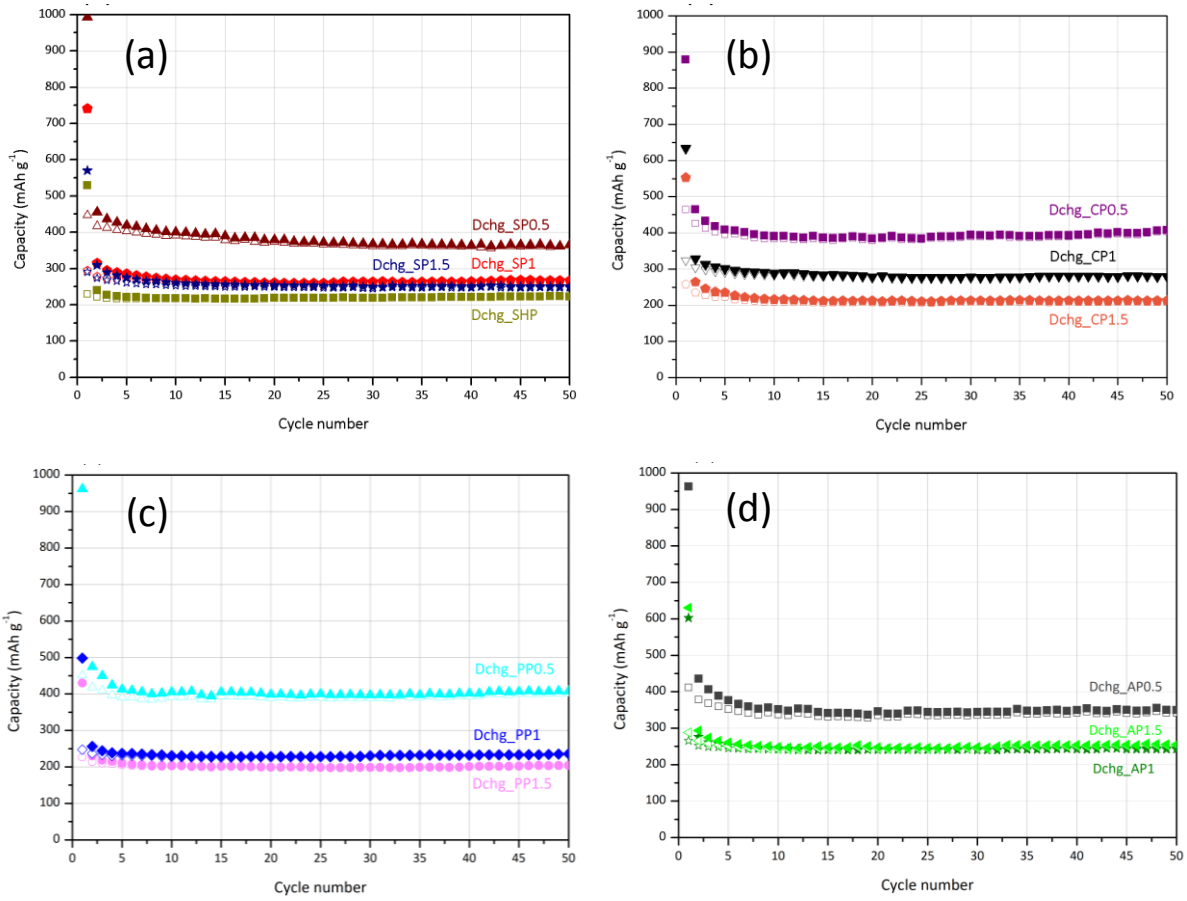

Fig. 7. Discharge/charge capacity as function of cycles for carbons derived from: **(a)** starch treated hydrothermally and ionothermally in three ILs ($FeCl_3$/BmimCl = 0.5, 1, 1.5); **(b)** chitosan; **(c)** pectin; and **(d)** alginic acid treated in three ILs ($FeCl_3$/BmimCl = 0.5, 1, 1.5). Electrodes formulation: active material, Super P (conductive carbon additive) and PVDF (binder) in the mass ratio of 80:10:10. Current density: 0.1 A g^{-1}. The specific capacities were calculated based on the mass of active material.

To further optimize the properties of these materials as negative electrodes in LIBs, the influence of the electrode formulation over electrochemical performance was studied. Thus, **CP1** electrodes were prepared using different binders (CMC *vs.* PVDF) and different slurry compositions (**Fig. S4**). On the one hand, CMC allowed reaching higher specific capacities than PVDF. This behaviour was already observed by Kim *et al.*[3] for polysaccharide-derived carbon electrodes. On the other hand, for the CMC series, increasing the mass ratio CA:**CP1** from 0:90 to 18:70 allowed increasing the reversible specific capacity of **CP1** by *c.a.* 80 %, *i.e.* from 200 to 360 mAh g^{-1} (after subtracting the capacity contribution from Super P, *ca.* 40 mAh g^{-1}, as its intrinsic specific capacity is of *ca.* 150 - 200 mAh g^{-1}).[36] A similar trend was observed with **CP0.5** (**Fig. 8**).

Considering the relatively high electronic conductivity of Super P (*c.a.* 280 S m^{-1})[37], this feature suggests that both **CP0.5** and **CP1** are probably still limited by their low intrinsic electronic conductivity.

The electrochemical performance of **CP0.5**, **CP0.5nw** and **CP0.5nw-HCl** were compared also using an electrode formulation AM:CA:CMC of 70:18:12,. Interestingly, the reversible specific capacity of **CP0.5** and **CP0.5nw** were very close (500 and 550 mAh g^{-1} respectively after 50 cycles; **Fig. 8**), while that obtained for **CP0.5nw-HCl** was more than 50 % lower (*c.a.* 200 mAh g^{-1} after 50 cycles). Thus, the presence of residual iron species, mainly Fe_3C and Fe(0), seems to prevail over the degree of graphitization in boosting the electrochemical performance.

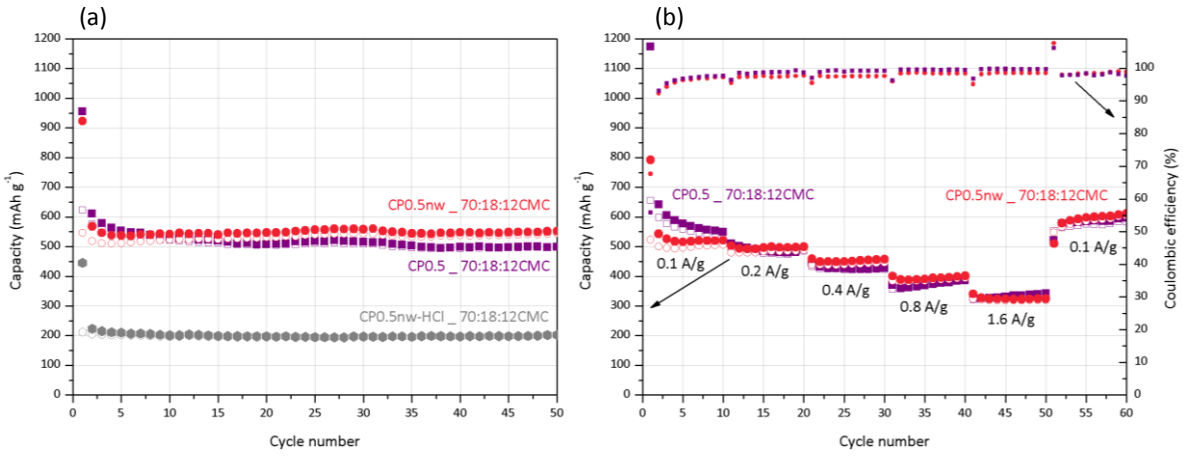

Fig. 8. (a) Cycling test of **CP0.5** (0.17 at.% Fe)‡, **CP0.5nw** (4.5 at.% Fe)‡ and **CP0.5nw-HCl** (1.0 at.% Fe)‡, **(b)** rate capability test and Coulombic efficiency of **CP0.5** (0.17 at.% Fe)‡ and **CP0.5nw** (4.5 at.% Fe)‡. The specific capacities were calculated based on the mass of active material. ‡According to SEM-EDX.

4. Conclusions

In this study, we have demonstrated that the ionothermal carbonization (ITC) of various polysaccharides in $FeCl_3$/BmimCl ionic liquids (ILs) can offer new opportunities for the preparation of carbon negative electrodes in Li-ion batteries (LIBs). We identified and varied several experimental parameters that allowed adjusting the chemical (nitrogen and iron content), the textural (specific surface area and pore volume) and the structural (degree of graphitization) properties of the as-obtained ionochars and carbon materials. We have

demonstrated that the $FeCl_3$/BmimCl molar ratio, which is related to the compactness and the thermal stability of ionic nanostructures in these ILs, is an important parameter allowing the tuning of the nanoporosity of the ionochars. We provided new insight into the influence of several important properties of the as-obtained carbon materials (*i.e.*, external pore volume, nitrogen functional sites, residual iron species and degree of graphitization) over their electrochemical performance. The best electrochemical performance was obtained for the carbons prepared from chitosan (*i.e.*, the carbon displaying the highest nitrogen content) and pre-treated in the ionic liquid with the lowest $FeCl_3$/BmimCl ratio (*i.e.*, 0.5) which yielded carbons with higher pore volumes. The presence of residual iron species, mainly Fe_3C and Fe(0), seems to prevail over the degree of graphitization in boosting the electrochemical performance. This work further highlights the versatility offered by the ionothermal approach for tayloring the textural, structural and electrochemical properties of carbon materials, with potential applications in the field of energy storage and conversion..

Conflicts of interest

There are no conflicts to declare.

Acknowledgements

Financial support was received by the European Commission in the framework of POROUS4APP project (H2020 GA no. 666157). The authors would like to thank Didier Cot (IEM, France) for SEM analyses, Erwan Oliviero (ICGM) for High resolution TEM analyses, Valérie Flaud (ICGM) for XPS analyses and Lea Daenens (ICGM) for technical help in the collection of the Raman spectra.

Notes and references

[1] Y. Yang, G.Y. Zheng, Y. Cui, Nanostructured sulfur cathodes, Chem Soc Rev 42(7) (2013) 3018-3032.
[2] A.D. Roberts, X. Li, H.F. Zhang, Porous carbon spheres and monoliths: morphology control, pore size tuning and their applications as Li-ion battery anode materials, Chem Soc Rev 43(13) (2014) 4341-4356.
[3] S. Kim, M. De Bruyn, J.G. Alauzun, N. Louvain, N. Brun, D.J. Macquarrie, L. Stievano, B. Boury, P.H. Mutin, L. Monconduit, Alginic acid-derived mesoporous carbonaceous materials (Starbon (R)) as negative electrodes for lithium ion batteries: Importance of porosity and electronic conductivity, J Power Sources 406 (2018) 18-25.
[4] M.M. Titirici, R.J. White, N. Brun, V.L. Budarin, D.S. Su, F. del Monte, J.H. Clark, M.J. MacLachlan, Sustainable carbon materials, Chem Soc Rev 44(1) (2015) 250-290.
[5] R.J. White, N. Brun, V.L. Budarin, J.H. Clark, M.M. Titirici, Always Look on the "Light" Side of Life: Sustainable Carbon Aerogels, Chemsuschem 7(3) (2014) 670-689.

[6] F. Yao, D.T. Pham, Y.H. Lee, Carbon-Based Materials for Lithium-Ion Batteries, Electrochemical Capacitors, and Their Hybrid Devices, Chemsuschem 8(14) (2015) 2284-2311.
[7] S. Dutta, A. Bhaumik, K.C.W. Wu, Hierarchically porous carbon derived from polymers and biomass: effect of interconnected pores on energy applications, Energ Environ Sci 7(11) (2014) 3574-3592.
[8] H. Lu, X.S. Zhao, Biomass-derived carbon electrode materials for supercapacitors, Sustainable Energy & Fuels 1(6) (2017) 1265-1281.
[9] Y.J. Heo, S.J. Park, H2O2/steam activation as an eco-friendly and efficient top-down approach to enhancing porosity on carbonaceous materials: the effect of inevitable oxygen functionalities on CO2 capture, Green Chem 20(22) (2018) 5224-5234.
[10] B. Hu, K. Wang, L.H. Wu, S.H. Yu, M. Antonietti, M.M. Titirici, Engineering Carbon Materials from the Hydrothermal Carbonization Process of Biomass, Adv Mater 22(7) (2010) 813-828.
[11] M.M. Titirici, M. Antonietti, Chemistry and materials options of sustainable carbon materials made by hydrothermal carbonization, Chem Soc Rev 39(1) (2010) 103-116.
[12] M.M. Titirici, A. Thomas, M. Antonietti, Back in the black: hydrothermal carbonization of plant material as an efficient chemical process to treat the CO2 problem?, New J Chem 31(6) (2007) 787-789.
[13] Y.C. Liu, B.B. Huang, X.X. Lin, Z.L. Xie, Biomass-derived hierarchical porous carbons: boosting the energy density of supercapacitors via an ionothermal approach, J Mater Chem A 5(25) (2017) 13009-13018.
[14] Z.L. Xie, R.J. White, J. Weber, A. Taubert, M.M. Titirici, Hierarchical porous carbonaceous materials via ionothermal carbonization of carbohydrates, J Mater Chem 21(20) (2011) 7434-7442.
[15] J.S. Lee, R.T. Mayes, H.M. Luo, S. Dai, Ionothermal carbonization of sugars in a protic ionic liquid under ambient conditions, Carbon 48(12) (2010) 3364-3368.
[16] T.P. Fellinger, A. Thomas, J.Y. Yuan, M. Antonietti, 25th Anniversary Article: "Cooking Carbon with Salt": Carbon Materials and Carbonaceous Frameworks from Ionic Liquids and Poly(ionic liquid)s, Adv Mater 25(41) (2013) 5838-5854.
[17] S.G. Zhang, K. Dokko, M. Watanabe, Carbon materialization of ionic liquids: from solvents to materials, Mater Horiz 2(2) (2015) 168-197.
[18] S.Y. Wu, Y.S. Ding, X.M. Zhang, H.O. Tang, L. Chen, B.X. Li, Structure and morphology controllable synthesis of Ag/carbon hybrid with ionic liquid as soft-template and their catalytic properties, J Solid State Chem 181(9) (2008) 2171-2177.
[19] H. Wang, G. Gurau, R.D. Rogers, Ionic liquid processing of cellulose, Chem Soc Rev 41(4) (2012) 1519-1537.
[20] R.P. Swatloski, S.K. Spear, J.D. Holbrey, R.D. Rogers, Dissolution of cellose with ionic liquids, J Am Chem Soc 124(18) (2002) 4974-4975.
[21] R.C. Remsing, R.P. Swatloski, R.D. Rogers, G. Moyna, Mechanism of cellulose dissolution in the ionic liquid 1-n-butyl-3-methylimidazolium chloride: a C-13 and Cl-35/37 NMR relaxation study on model systems, Chem Commun (12) (2006) 1271-1273.
[22] H. Zhang, J. Wu, J. Zhang, J.S. He, 1-Allyl-3-methylimidazolium chloride room temperature ionic liquid: A new and powerful nonderivatizing solvent for cellulose, Macromolecules 38(20) (2005) 8272-8277.
[23] M.S. Sitze, E.R. Schreiter, E.V. Patterson, R.G. Freeman, Ionic liquids based on FeCl3 and FeCl2. Raman scattering and ab initio calculations, Inorg Chem 40(10) (2001) 2298-2304.
[24] Z.L. Xie, X. Huang, M.M. Titirici, A. Taubert, Mesoporous graphite nanoflakes via ionothermal carbonization of fructose and their use in dye removal, Rsc Adv 4(70) (2014) 37423-37430.
[25] X.X. Lin, B. Tan, L. Peng, Z.F. Wu, Z.L. Xie, Ionothermal synthesis of microporous and mesoporous carbon aerogels from fructose as electrode materials for supercapacitors, J Mater Chem A 4(12) (2016) 4497-4505.
[26] P.F. Zhang, Y.T. Gong, Z.Z. Wei, J. Wang, Z.Y. Zhang, H.R. Li, S. Dai, Y. Wang, Updating Biomass into Functional Carbon Material in Ionothermal Manner, Acs Appl Mater Inter 6(15) (2014) 12515-12522.

[27] N. Zdolsek, A. Dimitrijevic, M. Bendova, J. Krstic, R.P. Rocha, J.L. Figueiredo, D. Bajuk-Bogdanovic, T. Trtic-Petrovic, B. Sljukic, Electrocatalytic Activity of Ionic-Liquid-Derived Porous Carbon Materials for the Oxygen Reduction Reaction, Chemelectrochem 5(7) (2018) 1037-1046.
[28] C. Falco, F.P. Caballero, F. Babonneau, C. Gervais, G. Laurent, M.M. Titirici, N. Baccile, Hydrothermal Carbon from Biomass: Structural Differences between Hydrothermal and Pyrolyzed Carbons via C-13 Solid State NMR, Langmuir 27(23) (2011) 14460-14471.
[29] C. Falco, N. Baccile, M.M. Titirici, Morphological and structural differences between glucose, cellulose and lignocellulosic biomass derived hydrothermal carbons, Green Chem 13(11) (2011) 3273-3281.
[30] M.M. Titirici, M. Antonietti, N. Baccile, Hydrothermal carbon from biomass: a comparison of the local structure from poly- to monosaccharides and pentoses/hexoses, Green Chem 10(11) (2008) 1204-1212.
[31] M. Thommes, K. Kaneko, A.V. Neimark, J.P. Olivier, F. Rodriguez-Reinoso, J. Rouquerol, K.S.W. Sing, Physisorption of gases, with special reference to the evaluation of surface area and pore size distribution (IUPAC Technical Report), Pure Appl Chem 87(9-10) (2015) 1051-1069.
[32] J.G. Li, Y.F. Hu, S.F. Sun, S. Ling, J.Z. Zhang, Ionic Structures of Nanobased FeCl3/[C(4)min]Cl Ionic Liquids, J Phys Chem B 116(22) (2012) 6461-6464.
[33] R. Gobel, Z.L. Xie, M. Neumann, C. Gunter, R. Lobbicke, S. Kubo, M.M. Titirici, C. Giordano, A. Taubert, Synthesis of mesoporous carbon/iron carbide hybrids with unusually high surface areas from the ionic liquid precursor [Bmim][FeCl4], Crystengcomm 14(15) (2012) 4946-4951.
[34] J.X. Wu, Z.Y. Pan, Y. Zhang, B.J. Wang, H.S. Peng, The recent progress of nitrogen-doped carbon nanomaterials for electrochemical batteries, J Mater Chem A 6(27) (2018) 12932-12944.
[35] Y. Ohtsuka, H. Mori, T. Watanabe, K. Asami, Nitrogen Removal during Atmospheric-Pressure Pyrolysis of Brown-Coal with Iron, Fuel 73(7) (1994) 1093-1097.
[36] K.A. See, M.A. Lumley, G.D. Stucky, C.P. Grey, R. Seshadri, Reversible Capacity of Conductive Carbon Additives at Low Potentials: Caveats for Testing Alternative Anode Materials for Li-Ion Batteries, J Electrochem Soc 164(2) (2017) A327-A333.
[37] S. Kim, A.M. Escamilla-Perez, M. De Bruyn, J.G. Alauzun, N. Louvain, N. Brun, D. Macquarrie, L. Stievano, B. Boury, L. Monconduit, P.H. Mutin, Sustainable polysaccharide-derived mesoporous carbons (Starbon (R)) as additives in lithium-ion batteries negative electrodes, J Mater Chem A 5(46) (2017) 24380-24387.